# A Comparison of Two Skip Entry Guidance Algorithms

Jeremy R. Rea*
*NASA Johnson Space Center, Houston, Texas, 77058, USA*
Zachary R. Putnam†
*The Charles Stark Draper Laboratory, Inc., Houston, Texas, 77058, USA*

**The Orion capsule vehicle will have a Lift-to-Drag ratio (L/D) of 0.3-0.35. For an Apollo-like direct entry into the Earth's atmosphere from a lunar return trajectory, this L/D will give the vehicle a maximum range of about 2500 nm and a maximum crossrange of 216 nm. In order to fly longer ranges, the vehicle lift must be used to loft the trajectory such that the aerodynamic forces are decreased. A Skip-Trajectory results if the vehicle leaves the sensible atmosphere and a second entry occurs downrange of the atmospheric exit point. The Orion capsule is required to have landing site access (either on land or in water) inside the Continental United States (CONUS) for lunar returns anytime during the lunar month. This requirement means the vehicle must be capable of flying ranges of at least 5500 nm. For the L/D of the vehicle, this is only possible with the use of a guided Skip-Trajectory. A skip entry guidance algorithm is necessary to achieve this requirement.**

**Two skip entry guidance algorithms have been developed: the Numerical Skip Entry Guidance (NSEG) algorithm was developed at NASA/JSC and PredGuid was developed at Draper Laboratory. A comparison of these two algorithms will be presented in this paper. Each algorithm has been implemented in a high-fidelity, 6 degree-of-freedom simulation called the Advanced NASA Technology Architecture for Exploration Studies (ANTARES). NASA and Draper engineers have completed several monte carlo analyses in order to compare the performance of each algorithm in various stress states. Each algorithm has been tested for entry-to-target ranges to include direct entries and skip entries of varying length. Dispersions have been included on the initial entry interface state, vehicle mass properties, vehicle aerodynamics, atmosphere, and Reaction Control System (RCS). Performance criteria include miss distance to the target, RCS fuel usage, maximum g-loads and heat rates for the first and second entry, total heat load, and control system saturation. The comparison of the performance criteria has led to a down select and guidance merger that will take the best ideas from each algorithm to create one skip entry guidance algorithm for the Orion vehicle.**

## Nomenclature

| | |
|---|---|
| $AFOM$ | Aerodynamic Figure-of-Merit |
| $ANTARES$ | Advanced NASA Technology Architecture for Exploration Studies simulation |
| $BSG$ | Big Sand Gap, Oregon |
| $CAP$ | CEV Aerosciences Project |
| $CAR$ | Carson Flats, Nevada |
| $CEV$ | Crew Exploration Vehicle |
| $CG$ | Center-of-Gravity |
| $CONUS$ | Continental United States |
| $C_D$ | Aerodynamic drag coefficient |
| $C_L$ | Aerodynamic lift coefficient |

*Aerospace Engineer, Flight Mechanics & Trajectory Design Branch, Mail Stop: EG5, AIAA Member.
†Staff Engineer, AIAA Member.

| | |
|---|---|
| $C_m$ | Aerodynamic pitching moment |
| $EAFB$ | Edwards Air Force Base, California |
| $EI$ | Entry Interface |
| $FPA$ | Flight Path Angle |
| $GRAM$ | Global Reference Atmosphere Model |
| $GN\&C$ | Guidance, Navigation, and Control |
| $GPS$ | Global Positioning System |
| $IMU$ | Inertial Measurement Unit |
| $ISS$ | International Space Station |
| $I_{xx}, I_{yy}, I_{zz}$ | Moments of Inertia |
| $I_{xy}, I_{xz}, I_{yz}$ | Products of Inertia |
| $JSC$ | Johnson Space Center |
| $LM606$ | Lockheed Martin 606 Orion Vehicle Configuration |
| $L/D$ | Aerodynamic lift-to-drag ratio |
| $NASA$ | National Aeronautics and Space Administration |
| $NSEG$ | Numerical Skip Entry Guidance |
| $RCS$ | Reaction Control System |
| $TPS$ | Thermal Protection System |
| $TRL$ | Technology Readiness Level |
| $UTTR$ | Utah Test Range, Utah |

# I. Introduction

From March to June 2007, engineers at NASA Johnson Space Center and Draper Laboratory conducted an entry guidance comparison for the Orion Crew Exploration Vehicle (CEV). This guidance comparison was motivated largely by the requirement for return to CONUS at anytime during the lunar month. The laws of physics dictates that in order to meet this requirement, the lunar return vehicle must be capable of a guided skip entry covering up to 5500 n.mi. of downrange. For a capsule-type vehicle with a lift-to-drag ratio (L/D) in the range of 0.3-0.35, this is only possible with a skip entry. As a guided skip entry has never been attempted with a crewed vehicle, this technology is at a low Technology Readiness Level (TRL). Two entry guidance algorithms were available; thus it was desired to determine which algorithm would be most robust to environment and navigation errors. The purpose of the exercise was not just to choose the most robust algorithm, but also to learn why certain methods worked better than others and to use this knowledge to improve and finally to merge the best ideas into one guidance algorithm.

# II. Skip Entry Guidance Algorithms

Two skip entry guidance algorithms were investigated during the course of this study. While this paper is not intended to describe each algorithm in detail, general descriptions of each algorithm are provided. Additional information on the algorithms is provided in the reference documents.

In general, each algorithm uses some form of numerical predictor-corrector for the skip phase coupled with the Apollo Final Phase Entry Guidance.[1,2] The Apollo Final Phase Entry Guidance is well documented and has been used successfully to return men from the Moon. The new technology development has been focused on the guided skip entry which commands the vehicle into a lofted trajectory, possibly exiting the atmosphere, in order to reach an energy state at a second Entry Interface (EI) point from which the Apollo Final Phase Guidance can safely return the vehicle to the landing target. In addition, all algorithms use some form of atmosphere and aerodynamic estimation; the nature of the numerical predictor-correctors made all the algorithms very sensitive to errors in these parameters.

## A. Numerical Skip Entry Guidance (NSEG)

Preliminary work on the NSEG algorithm was initiated in 1992 to assess long-range low L/D flight for the First Lunar Outpost.[3] Current major revisions to this algorithm combine features of the original high TRL Apollo Guidance algorithm with a numerical scheme for computing a real-time, long-range skip trajectory.

NSEG guides the vehicle to a point where the Apollo final-phase logic can take over at approximately Mach 23 and an altitude of approximately 200 kft. The Apollo final phase guides the vehicle to a point approximately 7 nmi from the landing site, at about Mach 1.6 and approximately 80-kft altitude.

### *1. NSEG Phases*

The NSEG algorithm is comprised of four main phases:

1. **Phase 1 (Numerical Predictor-Corrector):** Phase 1 begins at the first EI point. NSEG determines a bank command magnitude each guidance cycle by iteratively propagating constant-bank trajectories so that the predicted range-to-go at 160-kft altitude in the second entry converges to a desired reference range. NSEG evaluates the predicted range-to-go by propagating an in-plane trajectory (multiplying the lift coefficient by the cosine of the bank angle under consideration to get the in-plane contribution to lift, and ignoring the out-of-plane component). The predicted range-to-go is then calculated as the great circle range from the current navigated state to the landing site, minus the great circle range from the current navigated state to the terminal condition of the propagation. The out-of-plane motion is constrained to stay within a crossrange corridor to insure the vehicle flies to the desired target.

   Definition of the NSEG bank angle at any point in time is a one-dimensional search so that the range on the propagated trajectory matches the compensated reference range for the Apollo final phase guidance. Currently NSEG uses a bounded Regula-Falsi method to nominally find the solution. If difficulties are encountered such that a prediction is made outside of the bounded space, then the search switches to a half-step method to converge on a solution.

2. **Phase 2 (Blending):** During phase 2, a blended bank-angle command is used to transition the vehicle between the numerical solutions to the Apollo final phase solutions.

3. **Phase 3 (Apollo Final Phase):** Below an altitude of approximately 200-kft inbound on the second entry, the guidance enters phase 3 where the Apollo final phase logic is used exclusively. This guidance phase remains active until the vehicle planet relative speed drops below 1600 feet per second.

4. **Phase 4 (Proportional Steering):** Once the vehicle planet relative speed drops below 1600 feet per second, the proportional steering phase 4 is entered. A gain proportional to the heading error creates a bank command that guides the vehicle to the desired drogue deployment box. This drogue deployment box is comprised of altitude and range-to-target triggers.

Active in all phases except phase 4 is an enhanced Apollo lateral logic module that determines when the vehicle executes a roll reversal.

### *2. NSEG Aerodynamic and Atmospheric Estimation*

Two developments during NSEG development significantly increased the challenge facing skip-entry guidance: the anticipated CEV hypersonic lift-to-drag ratio (L/D) dropped from 0.40 to 0.35 to 0.30, and the CEV aero community mandated use of uniform distributions for aerodynamic lift coefficient ($C_L$), aerodynamic drag coefficient ($C_D$), and aerodynamic pitching coefficient ($C_m$) uncertainties. It became apparent that estimation of the actual CEV aerodynamic properties (using accelerometer data) was going to be necessary to meet the long range skip requirement with the desired reliability. An approach was developed whereby data derived from sensed lift and drag accelerations is averaged and filtered to independently update both the trim $C_L$ versus Mach number and trim $C_D$ versus Mach tables used by the NSEG propagator (the tables are defined for various values of hypersonic trimmed L/D).

It is important to note that the approach does not try to explicitly distinguish the individual effects of the aero uncertainties and atmospheric dispersions on the sensed accelerations. In fact, the approach also effectively compensates for atmospheric dispersions. The $C_L$ and $C_D$ are scaled exactly in proportion to the density deviation: the aerodynamic/atmospheric estimation approach is simply incorporating the density difference into the aero coefficients.

Results from the monte carlo and parametric stress tests of NSEG indicate this approach very effectively compensates for aerodynamic uncertainties and variations in the atmosphere. To accommodate very large dispersions, the $C_L$ and $C_D$ tables were extended far beyond the expected trim range of the CEV. The

intuitiveness of the technique suffers as a result of this extension (the coefficients are no longer easily related to a trim hypersonic L/D); a better approach might have been to use knowledge of the sensed L/D ratio to retain definition of more representative $C_L$ and $C_D$ values, while using a separate aero force scale factor to account for variations in atmosphere and mass.

## B. PredGuid

The PredGuid skip entry guidance algorithm combines the Apollo entry guidance algorithm with a modified version of the numerical predictor-corrector developed for the Aero-assist Flight Experiment aerocapture flight program. Specifically, PredGuid replaces the Down Control, Up Control, and Kepler phases of the Apollo guidance algorithm with a numerical predictor-corrector. This allows the PredGuid skip entry guidance algorithm to accurately target second entry conditions, providing significant long-range skip entry performance benefits over the original Apollo algorithm. After vehicle velocity has reached subsonic speeds, PredGuid employs a simple terminal guidance scheme to steer out remaining crossrange error. A complete description of the PRED GUID aerocapture algorithm can be found in Reference 4. A complete description of the original PredGuid skip guidance algorithm can be found in Reference 5.

### *1. PredGuid Phases*

PredGuid Skip Entry Guidance is composed of decoupled longitudinal/energy and lateral channels, as well as a simple terminal guidance scheme.

1. **Initial Roll:** This phase maintains proper vehicle orientation for entry and ensures atmospheric capture. This phase contains the Apollo entry guidance Pre-attitude Hold and Initial Roll phases. The Initial Roll phase has been modified to accommodate a user-specified initial bank angle instead of the full-lift-up orientation of the Apollo algorithm. This modification gives the user a measure of control over the shape and properties of the entry trajectory, including peak heat rate, integrated heat load, and peak deceleration. Capture into the atmosphere is assured through a command of full lift-down if the entry is deemed too shallow. The PredGuid Initial Roll phase begins at entry interface and terminates when the vehicle has reached an altitude rate of -700 ft/s.

2. **Energy Management:** The PredGuid Energy Management phase determines if a direct or skip entry is required, based on the specified target landing site range, and then guides the vehicle to the proper transition conditions for either Final phase (direct entry) or Up Control (skip entry). This phase utilizes the Apollo HUNTEST and Constant Drag phases with minor modifications. The vehicle controls its energy depletion during this phase while continuously computing the range to target with an analytic approximation. If a skip is required to reach the target, guidance transitions to Up Control when the range prediction error is less than 25 n.mi. If no skip is required, the vehicle transitions to Final phase when the proper velocity condition is reached.

3. **Up Control:** The guidance algorithm uses this mode if a skip entry is required to achieve the desired target range. This phase replaces the Apollo Down Control and Up Control phases. During this phase, the numerical predictor-corrector is active. PredGuid's predictor-corrector integrates simplified equations of motion to determine a constant bank angle trajectory that will achieve the desired range at the proper velocity-flight-path angle ($V$,$\gamma$) conditions for Final phase start at second entry. PredGuid uses a unique corrector method to find a solution to the constant bank angle trajectory problem. First, the predictor is used to propagate the vehicle trajectory to the appropriate ($V$,$\gamma$) Final phase conditions. If the calculated range over this propagation is within a given tolerance, the constant bank angle used to generate the trajectory is output to flight control. If the range is not within the tolerance, the corrector determines a new bank angle and the predictor is run again. This phase terminates when the vehicle exits the sensible atmosphere, defined to be when vehicle drag drops below 6.0 ft/s$^2$.

4. **Ballistic:** This phase corresponds to the exo-atmospheric skip portion of skip entry and replaces the Apollo Kepler phase. The purpose of this phase is to maintain proper vehicle attitude during exo-atmospheric flight. The predictor-corrector continues to run through this phase, but no commands are issued to flight control when vehicle acceleration is less than 1.6 ft/s$^2$. This prevents guidance from using fuel in a flight regime in which the vehicle has limited control authority. This phase terminates

when the vehicle reenters the sensible atmosphere, when the drag rises above 6.5 ft/s2. This drag trigger is intentionally set higher than the atmospheric exit trigger to ensure proper phase transition between Up Control and Ballistic.

5. **Final:** PredGuid uses the Apollo Final phase guidance logic for direct and second entry. The Apollo Final phase is a reference-following guidance algorithm that guides the vehicle from circular to subsonic velocity. PredGuid uses the Final phase in conjunction with an updated reference trajectory appropriate for use with the LM606 CM and skip entry. This phase terminates when the Earth-relative vehicle velocity reaches a magnitude of 1000.0 ft/s.

6. **Terminal Guidance:** The terminal guidance phase is used to fly out remaining crossrange error after the Final phase concludes. A simple proportional guidance scheme is used to steer the vehicle based on a heading error proxy generated by Apollo Lateral Logic. This phase terminates when the specified drogue deploy conditions are reached.

PredGuid uses a de-coupled lateral channel to manage crossrange throughout entry. The PredGuid lateral channel guidance is identical to that of the Apollo Lateral Logic, with a modified lateral corridor definition. The lateral channel uses bank reversals to manage crossrange and heading errors. The lateral channel is active from entry interface until the end of the Final phase at 1000 ft/s.

*2. PredGuid Aerodynamic and Atmospheric Estimation*

PredGuid uses navigated acceleration and velocity, in conjunction with stored parameters, to estimate the current vehicle L/D and a density correction factor. The nominal vehicle L/D is used as an initial value. The value current estimate is bounded to ensure a reasonable estimate and then filtered with previous estimates to reduce transient effects. The L/D estimator is active only during the Energy Management and Up Control phases.

PredGuid also estimates a density correction factor to account for day-of-flight atmospheric conditions. This factor is calculated as a ratio with the on-board atmospheric model density. The ratio is bounded between a maximum and minimum value and averaged with previous estimates. The density estimator assumes that the drag coefficient remains close to its nominal value throughout the flight and that the L/D estimate is accurate. The density estimator is active when the vehicle acceleration magnitude is greater than 2.0 ft/s$^2$.

## III. Guidance Comparison Definition

This section describes the mechanics of the comparison between the two guidance algorithms.

### A. Guidance Comparison Phases

The comparison was carried out in two phases. Phase 1 established the baseline performance comparison between the guidance algorithms. The guidance Principal Investigators were then permitted to make modifications to optimize the performance of each guidance algorithm. These optimization approaches were openly discussed during the Skip-Entry weekly guidance team meetings, and guidance logic was freely distributed between the guidance groups. Therefore, Phase 2 facilitated a comparison and an effective merging of the strengths of the guidance systems. In reality the actual exchange of code was minimal. This was due to significant differences in the structure of the guidance algorithms. However, free exchange of ideas and approach techniques directed the optimization efforts of Phase 2. Phase 2 then executed the same suite of comparison runs to establish a final optimized set of performance comparison data sets. At the end of Phase 2 Merger, a Selection Board of GN&C experts was assembled to evaluate the data and recommend the primary and backup guidance algorithms to support the Orion program.

### B. Vehicle Configuration

The Lockheed Martin 606 (LM606) Orion configuration[8] was chosen as the baseline configuration for purposes of the guidance comparison. This vehicle has a nominal hypersonic lift-to-drag ratio of 0.35. The other details will be left to the reference.

### C. Entry Interface (EI) States and Landing Sites

Five lunar return EI states were chosen as reference points for the comparison. Each of the five EI states represents a lunar return state with a different downrange, crossrange, and azimuth angle to the continental United States (CONUS). For each EI state, one primary landing site and two weather alternate landing sites were chosen. Figure 1 defines the EI states and the landing site triplets for each state. The primary landing site for each EI state is Edwards Air Force Base, California (EAFB). The Utah Test Range, Utah (UTTR) is a weather alternate site for all the EI states. For EI state 1, the third site is Big Sand Gap, Oregon (BSG). For all the other EI states, the third landing site is Carson Flats, Nevada (CAR). It should be noted that actual landing sites for the Orion program have not yet been chosen. The landing sites listed in this paper were used solely as representative of the downrange and crossrange variations that may be seen for a lunar return mission during the Orion program.

| EI Condition | EI Site 1 | EI Site 2 | EI Site 3 | EI Site 4 | EI Site 5 |
|---|---|---|---|---|---|
| Geodetic Latitude | -46.5° | -26.2869 ° | -6.98043 ° | 15.6016 ° | 19.68 ° |
| Longitude | -112.552 ° | -113.805 ° | -150.113 ° | -171.51 ° | -146.523 ° |
| Geodetic Altitude (ft) | 400,000 | 400,000 | 400,000 | 400,000 | 400,000 |
| Inertial Velocity (fps) | 36046 | 36046 | 36046 | 36046 | 36046 |
| Inertial Flightpath | -5.86 ° | -5.86 ° | -5.86 ° | -5.86 ° | -5.05 ° |
| Inertial Azimuth | 0 ° | 0 ° | 32.2642 ° | 55.9743 ° | 47.794 ° |
| Inclination | 90 ° | 90 ° | 58 ° | 37 ° | 46 ° |
| Range to Targeted Landing Site (n.mi) | 5220 - UTTR<br>**4880 - EAFB**<br>**5330 – BSG** | 4010 - UTTR<br>**3660 - EAFB**<br>3960 - CAR | 3640 - UTTR<br>**3230 - EAFB**<br>3440 - CAR | 3540 - UTTR<br>**3290 - EAFB**<br>3300 - CAR | 2160 - UTTR<br>1820 - EAFB<br>1940 - CAR |
| Crossrange to Targeted Landing Site (n.mi) | 250 - UTTR<br>**30 - EAFB**<br>**25 – BSG** | 240 - UTTR<br>**20 - EAFB**<br>16 - CAR | 140 - UTTR<br>**220 - EAFB**<br>8 - CAR | -220 - UTTR<br>**100 - EAFB**<br>-194 - CAR | -25 - UTTR<br>155 - EAFB<br>-85 - CAR |

**Figure 1. Reference Entry Interface States**

### D. Guidance Comparison Metrics

Each guidance algorithm underwent an identical set of monte carlo and parametric stress testing in several areas to assess performance capability for nominal, monte carlo, and parametrically dispersed flight conditions. Data was compiled to facilitate performance comparisons. The metrics used were:

- **Target Landing Site Accuracy:** Each guidance algorithm was assessed in terms of reaching within 2.7 n.mi. (5 km) of the desired target landing sites. Three landing sites were targeted from each of the five EI Sites. The target for each of these sites was a drogue deployment "box" fixed at a ground altitude between 35,000 and 45,000 feet altitude above the reference ellipsoid at the desired landing point. No wind biasing of the target was attempted in this study. Although the primary accuracy objectives of the guidance algorithms was to accurately achieve the drogue deployment box, the trajectories were integrated to a ground landing point using drogue and main parachute models.

- **Fuel Consumption:** Reaction Control System (RCS) jets were fired during the atmospheric and exo-atmospheric Skip-Entry flight phases to control the vehicle attitude. While in the atmosphere the RCS jets were used to direct the vehicle lift acceleration while the vehicle was aerodynamically trimmed in pitch. Outside the atmosphere the RCS jets were again used to provide 3-axis control of the vehicle and prepare for second entry. No exo-atmospheric correction maneuvers were used in any part of the analysis in this report. Although an exo-atmospheric correction maneuver can be used to remove errors accumulated during the first skip maneuver, the cost in terms of propellant makes this an undesirable maneuver. Accurately achieving the landing site targets without using correction maneuver RCS propellant is a highly desirable result for Skip-Entry flight. Minimizing vehicle attitude control system fuel requirements is an important metric for evaluating relative guidance system performance.

- **Total Heat Load:** The long ranges flown by the Skip-Entry vehicle result in a high integrated heat load. The increased heat load resulting from Skip-Entry, as opposed to a Direct Entry flight, results in increased Thermal Protection System (TPS) mass. The TPS insulation must be properly sized to accommodate the greatest heat load experienced by the vehicle. This occurs for the longest range flights. Metrics comparing the relative convective and radiative heating were compiled throughout this analysis to determine performance differences affecting TPS mass using the different guidance algorithms. However, the trajectory design cannot be done oblivious to peak heat rates which may drive TPS shear concerns with ablator, so data was also gathered on peak heat rates during flight.

- **Maximum Acceleration and Durations:** A significant difference in Skip-Entry flight design from Direct Entry flight design is the necessity to significantly loft the trajectories. This lofting enables the high ballistic number, low L/D vehicle to travel large downranges and crossranges. However, this entails a double peak in sensed acceleration. On a long range Skip-Entry trajectory, the crew will experience a substantial period of low sensed acceleration following the first entry. Understanding and quantifying these loads is important for proper design of the CEV structure, as well as understanding how the crew will participate in monitoring, command, and control during the flight.

- **Robustness:** Individually varying dispersion sources outside of the expected range of uncertainty provides a useful metric for determining the relative performance of the guidance algorithms. Assessing the sensitivity of each guidance to variations in models and systems will drive confidence metrics. Parametric studies were completed to test for robustness to variation in environment and navigation states.

- **Complexity:** A guidance algorithm requires a set of initialization parameters called I-Loads. Assessing the I-Load reconfiguration requirements for the guidance algorithms is a useful comparative metric. Also determining the sensitivity of the guidance algorithms to hardware lags and understanding simulation code complexity are helpful metrics of comparison.

### E. Simulation Testbed

The Advanced NASA Technology Architecture for Exploration Studies (ANTARES) was used to evaluate the skip guidance algorithms. ANTARES is a six degree-of-freedom simulation tool that provides a realistic simulation environment. It is comprised of a library of vehicle generic models and vehicle specific models defined for the Orion vehicle. ANTARES includes high-fidelity models of the navigation system, control system, vehicle mass properties, vehicle aerodynamics, atmosphere and winds, gravitational, and aerothermal environment. It is currently configured for phase-specific simulations - ascent, on-orbit, and entry. For this analysis, the ANTARES Entry simulation was used. While the ANTARES simulation is constantly improving, ANTARES V07.1.0 was used for the analysis of the skip guidance algorithms. More information on the Entry, Descent, and Landing capability of ANTARES can be found in Reference 7.

### F. Monte Carlo Analysis

Skip entry monte carlo flight performance was evaluated using the technique of monte carlo analysis. One monte carlo set consisted of 3000 trajectories with parameters randomly dispersed over the range of possible dispersed conditions shown in Table 1. Different vehicle L/D's and EI flight path angles (FPAs) were evaluated in this report to determine their effect on relative guidance performance. A 15-set monte carlo run matrix is defined as one 3000 case monte carlo run for each combination of the 5 EI states and 3 possible landing sites. Three of these 15-set monte carlo run matrices were generated for each guidance algorithm. One set was for a hypersonic L/D of 0.35, with an EI FPA of -5.86° for EI States 1-4, another for L/D 0.30 and an EI FPA of -5.86°, and another for L/D 0.30 and an EI FPA of -5.75°. Note that all EI State 5 cases use an EI FPA of -6.05° to represent a "planned" shorter range lunar return.

### G. Parametric Stress Analysis

Several parametric variations were performed where a particular set of parameters was varied far beyond their expected dispersed values. This section describes each parametric analysis.

**Table 1. Monte Carlo Dispersions.**

| Parameter | Dispersion | Mean | 3-Sigma or Min/Max |
|---|---|---|---|
| EI Altitude | Uniform | 400,000 ft | ± 500 ft |
| EI Latitude/Longitude | Uniform | Varies | ± 0.2° |
| EI Velocity | Gaussian | 36,046 ft/sec | 90 ft/sec |
| EI Flight Path Angle | Gaussian | Varies | 0.1° |
| EI Azimuth | Uniform | Varies | ± 0.05° |
| Atmosphere and Winds | GRAM-99 model seed | – | – |
| Aerodynamic Coefficients | Defined by CAP team[9] | – | Varies |
| Vehicle Mass | Uniform | LM606 configuration[8] | ± 3.1% |
| Vehicle Center-of-Mass | Gaussian | LM606 configuration | 0.5 inches - Xcg<br>0.3 inches – Ycg, Zcg |
| Vehicle Inertia | Gaussian | LM606 configuration | 10% - Ixx, Iyy, Izz<br>50% - Ixy, Ixz, Iyz<br>(correlated seeds) |
| RCS Thrust | Uniform | 160 lbf | ± 5% |
| GPS Noise | Gaussian | – | Model seed |
| IMU Noise | Gaussian | – | Model seed |
| IMU Alignment Position | Uniform | Varies | ± 0.1 inches |
| IMU Alignment Attitude | Uniform | Varies | ± 20 arc sec |

### 1. *Footprint*

An investigation of the nominal landing footprint capability of each algorithm was completed. The footprints were generated using EI state 1 as the initial condition, an EI bank angle of 0°, an EI flight path angle of -5.86°, and an L/D = 0.35. The geodetic latitude of the landing site was varied from -30° to 70° at 5° increments. The longitude of the landing site was varied from -132.552° to -122.552° at 0.5° increments. This opens the footprint at a downrange of 1000 n.mi. and closes it at a downrange of roughly 7000 n.mi. All other parameters were held at their nominal values.

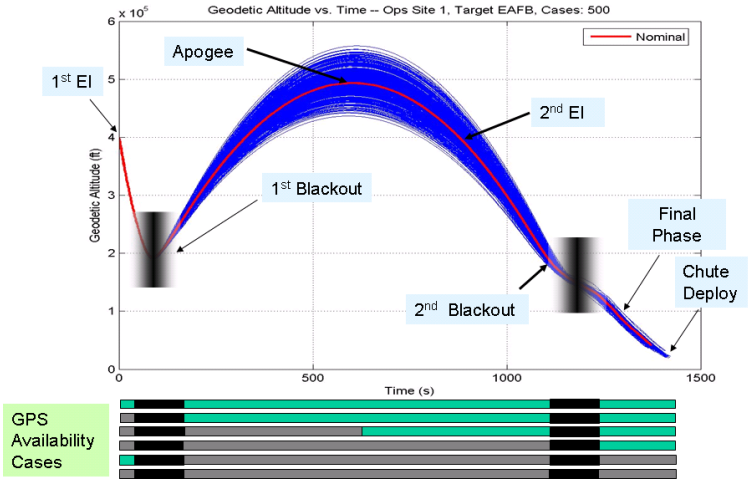


**Figure 2. GPS Availability Scenarios**

### 2. *EI State*

The sensitivity to EI state dispersions was investigated for each algorithm. The data was generated using EI state 1 as the initial condition, BSG as the landing site, an EI bank angle of 0°, and an L/D = 0.35. The EI inertial flight path angle was varied from -7.36° to 4.36° at 0.05° increments. The EI inertial azimuth was varied from -14° to 10° at 0.4° increments. All other parameters were held at their nominal values.

*3. Navigation*

Sensitivities to various navigation system parameters were investigated for each algorithm. The data was generated using EI state 1 as the initial condition, BSG as the landing site, an EI flight path angle of -5.86°, and an L/D = 0.35.

In order to test the effects of Global Positioning System (GPS) availability on the guidance response, six GPS availability scenarios were identified (see Figure 2). The GPS blackout is modeled when the drag acceleration is above 0.5 $m/s^2$ and the altitude is above 180,000 feet. This allows the GPS measurements to be used during the exo-atmospheric skip and for the lower portion of the second entry. Two black-out periods typically occur during a skip entry. The six GPS availability scenarios are:

1. 1B1B1: GPS ON - Blackout - GPS ON - Blackout - GPS ON
2. 0B1B1: GPS OFF - Blackout - GPS ON - Blackout - GPS ON
3. 0B01B1: GPS OFF - Blackout - GPS OFF - GPS ON @ Apogee - Blackout - GPS ON
4. 0B0B1: GPS OFF - Blackout - GPS OFF - Blackout - GPS ON
5. 1B0B0: GPS ON - Blackout - GPS OFF - Blackout - GPS OFF
6. 0B0B0: GPS OFF - Blackout - GPS OFF - Blackout - GPS OFF

For GPS availability scenarios that have GPS at EI (all cases that begin with "1"), it was assumed that GPS was available previous to EI. For GPS availability scenarios that do not have GPS at EI (all cases that begin with "0"), it was assumed that GPS was not available previous to EI. For each of these possibilities, a covariance matrix was used to define the correlated position/velocity navigation errors at EI. Note that due to this assumption, EI navigation errors are larger for the no-GPS-at-EI cases than for the cases that initially had GPS.

- **Reduced Set Monte Carlos**

  Reduced set monte carlos were run for each GPS availability scenario. A reduced set Monte-Carlo is defined as the first 100 cases of the full 3000 case monte carlo set.

- **Parametric Sweep on Navigation Position/Velocity Error at EI**

  It is possible to apply a scale factor to the position/velocity navigation error covariance matrix. This has the effect of increasing/decreasing the state navigation error. This factor can be thought of as a sigma multiplier. When it has an absolute value of 1, the correlated error is 1-sigma. An absolute value of 2 gives a correlated error of 2-sigma, and etcetera. In addition, a sign (+/-) can be applied in order to change the sense of this error. The sigma multiplier was varied from -20 to 20 at an increment of 0.1.

- **Parametric Sweep on Navigation Attitude Error at EI**

  The navigation attitude error on the body-to-inertial Euler angles (roll, pitch, and yaw) can be manipulated by use of a scale factor. This scale factor was varied from -1 to 1 at increments of 0.01.

- **Parametric Sweep on Navigation Acceleration Bias**

  The un-estimated accelerometer bias in each axis of the Inertial Measurement Unit (IMU) was varied. A multiplier was applied to the bias found in the standard specifications for the IMU model. This multiplier was varied from -0.5 to 0.5 at increments of 0.005.

*4. Mass Properties*

A study of the sensitivities of each guidance algorithm to variations in mass and center-of-gravity (CG) was completed. The data was generated using EI state 1 as the initial condition, BSG as the landing site, an EI flight path angle of -5.86°, and an L/D = 0.35.

- **Mass**

  The mass was varied from 10,369.2 lbm to 30,369.2 lbm (50%-150% of its nominal value of 20,369,2 lbm) at 100 lbm increments. All other parameters were held at their nominal values.

- **Center-of-Gravity (CG)**

  The Y-body CG location was varied from -4.9 inches to 5.1 inches at 0.5 inch increments. The Z-body CG location was varied from 3.2 inches to 13.2 inches at 0.5 inch increments. All other parameters were held at their nominal values.

*5. Atmosphere*

Atmospheric variations were found to be a potential major source of error for the guidance algorithms. A sensitivity study was completed to determine how sensitive each algorithm was to atmospheric perturbations. The data was generated using EI state 1 as the initial condition, BSG as the landing site, an EI flight path angle of -5.86°, and an L/D = 0.35.

In order to capture the effects of monthly density variations, reduced set monte carlos were run for each month. As mentioned earlier, a reduced set monte carlo is defined as the first 100 cases of the full 3000 case monte carlo set. In addition to the monthly variation, the magnitude of all dispersions was varied. The Global Reference Atmosphere Model (GRAM) 99 V3 is implemented in the ANTARES simulation. In GRAM-99 V3, there is a scale factor called RPSCALE. This is a scale factor on the 1-sigma variation about the nominal atmospheric parameters (i.e. density, pressure, speed of sound, wind magnitude, etc.). The nominal value of RPSCALE is 1.0. In order to expose each guidance algorithm to stressful atmospheric dispersions, the RPSCALE factor was varied to values of 1.0, 1.5, and 2.0. Thus, at RPSCALE = 2.0, the 1-sigma dispersion variation was effectively doubled about the nominal atmosphere.

*6. Control*

Sensitivity to control system parameters was investigated for each guidance algorithm. The data was generated using EI state 1 as the initial condition, BSG as the landing site, an EI flight path angle of -5.86°, and an L/D = 0.35.

- **RCS Thrust Magnitude**

  The RCS thrust magnitude was varied from 20 lbf to 500 lbf at 20 lbm increments. All other parameters were held at their nominal values.

- **Control System Lag**

  The control system lag time between guidance commanded attitude and control response was varied from 0 sec to 0.68 sec at 0.04 sec increments. All other parameters were held at their nominal values.

*7. Aerodynamics*

Aerodynamic dispersions were found to be a major disturbance to the guidance algorithms. As such, a study was completed to test the sensitivity of each algorithm to variations in the aerodynamics of the vehicle. The data was generated using EI state 1, 2, 3, 4, and 5 as initial conditions, EAFB as the landing site, and an EI flight path angle of -5.86°. The nominal center-of-gravity for LM606 was used.

The aerodynamic data base[9] gives aerodynamic uncertainties as 3-sigma values about the nominal. These uncertainties are multiplied by a factor and added to the nominal. Equation 1 below shows the basic implementation of the aerodynamic uncertainties. This formulation is documented in Reference 10. The uncertainties can be a function of Mach number, angle of attack, and possibly other parameters.

$$C_L = C_{L_{nominal}} + U_{C_L} * factor \tag{1}$$

where:

$U_{C_L}$ = 3-sigma uncertainty
$factor$ = Uncertainty multiplier

A sweep on the uncertainty multiplier for $C_L$, $C_D$, and $C_m$ was completed. The uncertainty multiplier on $C_m$ was varied at values of -2, -1, 0, 1, 2. For each value of the $C_m$ uncertainty multiplier, the uncertainty multipliers for $C_L$ and $C_D$ were then varied as:

- $C_L$ uncertainty multiplier varied from -20 to 30 at increments of 1
- $C_D$ uncertainty multiplier varied from -20 to 20 at increments of 1

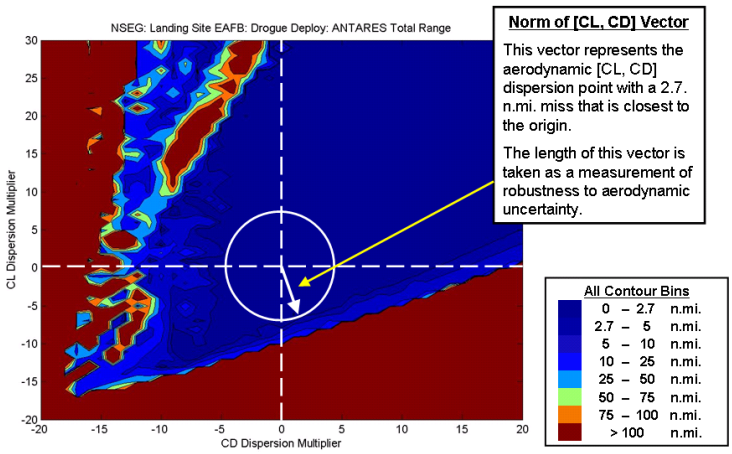


**Figure 3. Definition of the Aerodynamic Figure-of-Merit (AFOM)**

Figure 3 shows an example of the figure-of-merit used to describe the sensitivity to the aerodynamics. The colors represent the total range-to-target at the drogue deploy condition for a given set of $C_L$ and $C_D$ uncertainty multipliers; the plot is for one value of $C_m$ uncertainty multiplier. The white arrow points from the origin to the nearest approach of the 2.7 n.mi. miss line to the origin. The length of this arrow is the Aerodynamic Figure-of-Merit (AFOM).

# IV. Results

This section covers some of the multitudinous volumes of data that was created during the course of the guidance comparison activity. It is not possible to cover all results in the format of this paper.

## A. Phase I Results

The Phase I results were used to improve NSEG and PredGuid. They will not be presented here in favor of the Phase II results presented in the next section.

## B. Phase II Results

### *1. Monte Carlo Results*

This section presents example results of the monte carlo analyses. Figures 4 and 5 show the landing accuracy and RCS propellant usage for each guidance algorithm flying from EI state 1 to BSG with an L/D = 0.3 and EI FPA = -5.86°. NSEG results are blue circles while PredGuid results are red crosses. Note that PredGuid hits the target with higher precision at the cost of more average RCS fuel usage. Figures 6 and 7 show the maximum sensed accelerations for the first and second entries. It can be seen that PredGuid flies with a lower maximum sensed acceleration during the second entry.

Figures 8 through 11 show time history plots of various trajectory parameters. These plots give an insight into how the skip guidance algorithms operate under dispersed conditions. Each figure shows the nominal trajectory in red, with the 3000 dispersed Monte Carlo trajectories in blue. In each figure, the top subplot shows the NSEG trajectories and the bottom subplot shows the PredGuid trajectories. All of the following plots are for a vehicle with L/D=0.35 flying from EI state 1 to EAFB with an EI FPA of -5.86°. Figure 8 shows a plot of actual bank angle versus planet relative velocity magnitude. Figure 9 shows the geodetic altitude time history. Figure 10 shows actual crossrange versus downrange. Figure 11 shows a time history of dynamic pressure.

### *2. Footprint*

The following plots show the landing footprint capability of each algorithm. In Figure 12, the colors represent the total range-to-target at the drogue deploy condition for a given landing site. In Figure 13, the 2.7 n.mi.

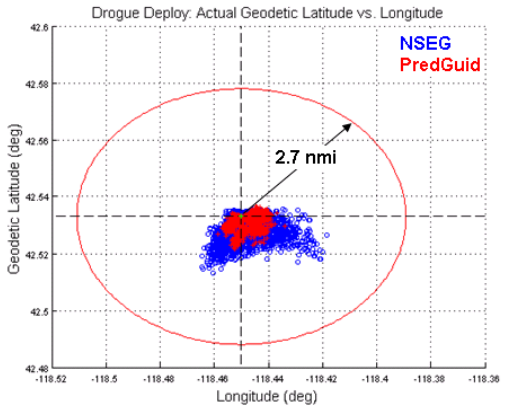


**Figure 4. Accuracy at Drogue Deploy: L/D 0.30, EI FPA -5.86°, EI1-to-BSG**

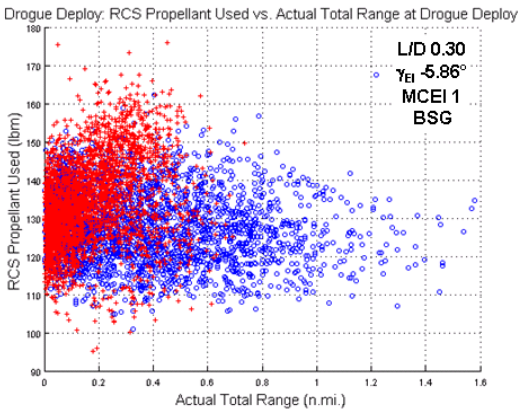


**Figure 5. RCS Prop Usage vs. Drogue Deploy Miss Distance: L/D 0.35, EI FPA -5.86°, EI1-to-EAFB**

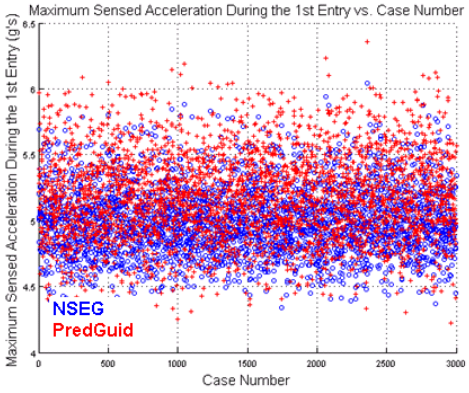


**Figure 6. Maximum Sensed Acceleration in 1st Entry: L/D 0.30, EI FPA -5.86°, EI1-to-BSG**

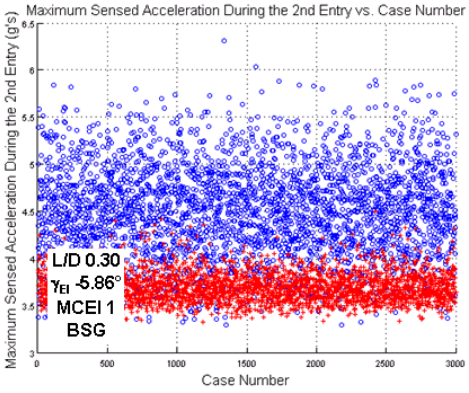


**Figure 7. Maximum Sensed Acceleration in 2nd Entry: L/D 0.30, EI FPA -5.86°, EI1-to-BSG**

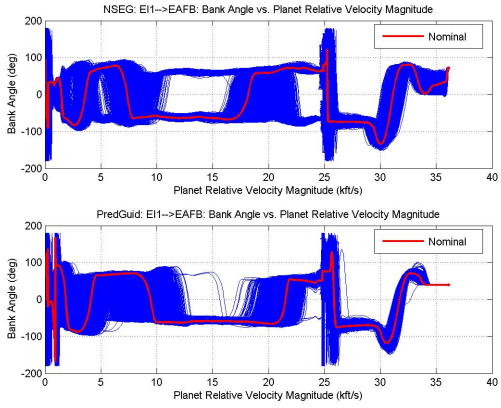


**Figure 8. Bank Angle vs. Planet Relative Velocity: L/D 0.35, EI FPA -5.86°, EI1-to-EAFB**

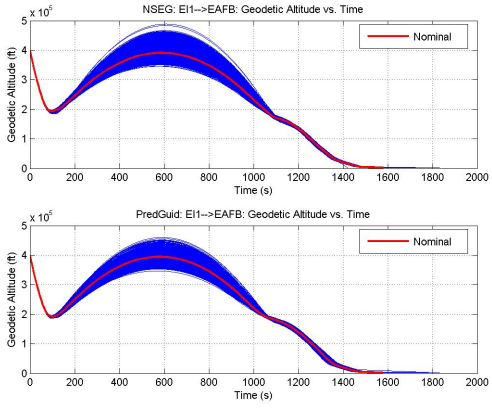


**Figure 9. Geodetic Altitude vs. Time: L/D 0.35, EI FPA -5.86°, EI1-to-EAFB**

miss line and the 100 n.mi. miss line for each algorithm are co-plotted for easier comparison. Note that the shape of the footprint is skewed in favor of negative crossrange. In this case, the initial azimuth was flying

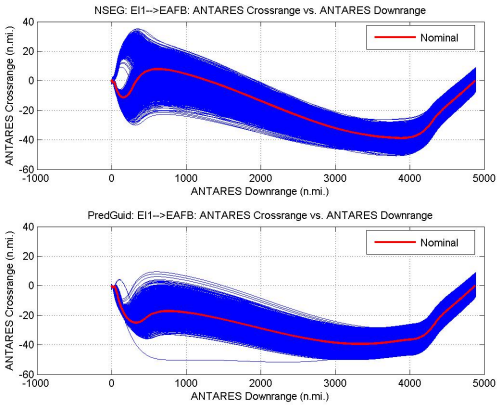


**Figure 10. Crossrange vs. Downrange: L/D 0.35, EI FPA -5.86°, EI1-to-EAFB**

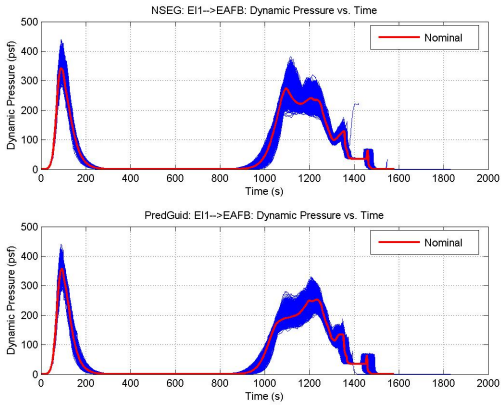


**Figure 11. Dynamic Pressure vs. Time: L/D 0.35, EI FPA -5.86°, EI1-to-EAFB**

due North. Thus, the footprint skew is due to the rotation of the Earth beneath the vehicle. It can be seen that PredGuid has a slightly larger footprint that NSEG.

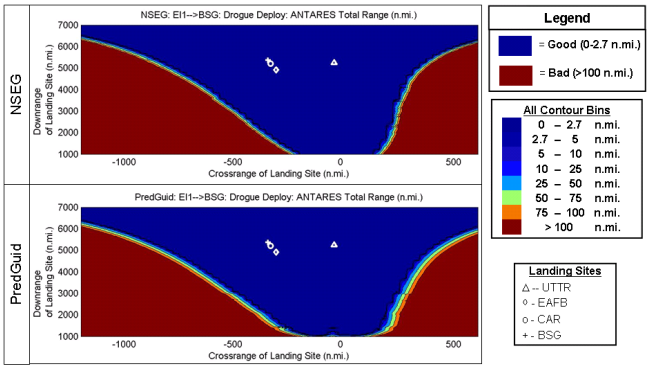


**Figure 12. Footprint**

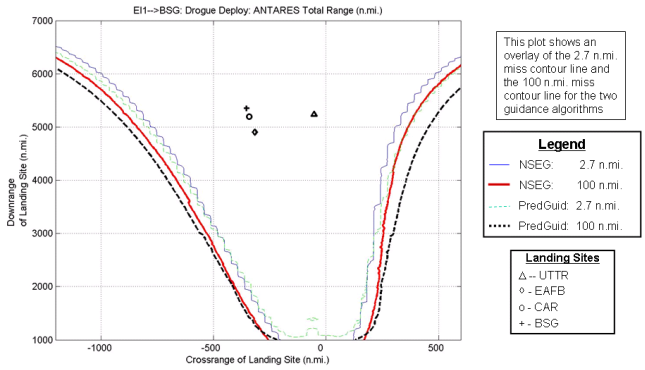


**Figure 13. Footprint Comparison**

### *3. EI State*

The following plots show the sensitivity to EI state dispersions for each algorithm. In Figure 14, the colors represent the total range-to-target at the drogue deploy condition for a given EI flight path angle and azimuth. In Figure 15, the 2.7 n.mi. miss line and the 100 n.mi. miss line for each algorithm are co-plotted for easier comparison. Note that both algorithms reach a skip out point at EI FPAs above -4.8°. Also, note that PredGuid has a red band of misses. This band did not occur during the Phase I comparison runs. The reasons for its existence in Phase II are under investigation.

### *4. Navigation*

- **Reduced Set Monte Carlos**

  Reduced set monte carlos were run for each GPS availability scenario. A reduced set monte carlo is defined as the first 100 cases of the full 3000 case monte carlo set. The results are given in Figure 16. Note that the GPS availability scenario case with no GPS for the entire trajectory (lower right hand corner) produces more misses.

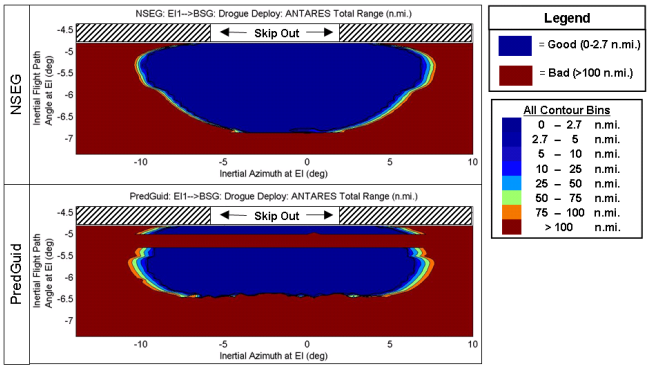


**Figure 14. EI State Sensitivity**

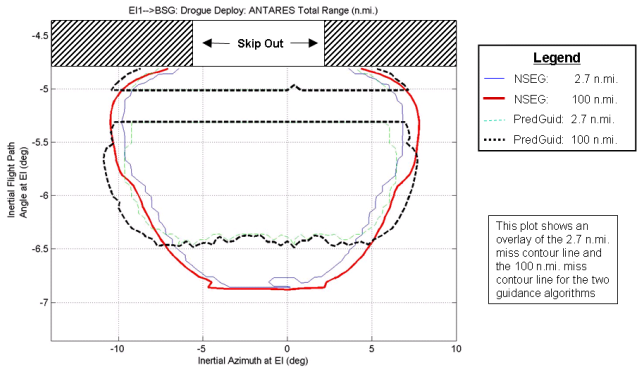


**Figure 15. EI State Sensitivity Comparison**

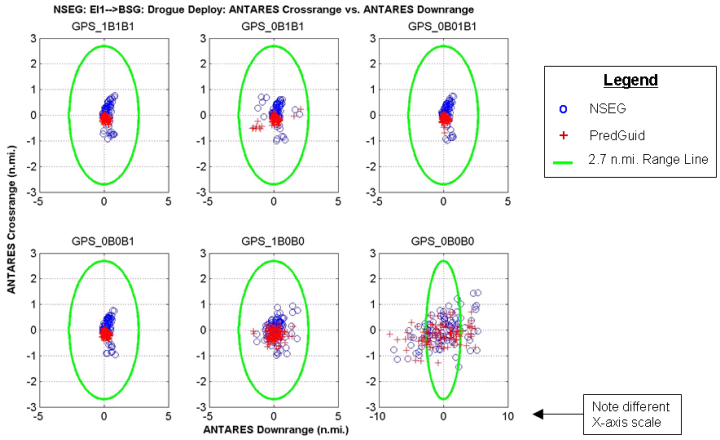


**Figure 16. Reduced Set Monte Carlos for GPS Availability Scenarios**

- **Parametric Sweep on Navigation Position/Velocity Error at EI**

  Figure 17 shows the total range-to-target at the drogue deploy condition as a function of the navigated position/velocity error sigma multiplier for each algorithm. Figures 18 shows a zoomed in view of the same data. From the figures it can be seen that NSEG is less sensitive to this parameter than PredGuid.

- **Parametric Sweep on Navigation Attitude Error at EI**

  Figure 19 shows the total range-to-target at the drogue deploy condition as a function of the navigated attitude error multiplier for each algorithm. Figures 20 shows a zoomed in view of the same data. It can be seen that PredGuid is slightly less sensitive to the navigation attitude error than NSEG.

- **Parametric Sweep on Navigation Acceleration Bias**

  Figure 21 shows the total range-to-target at the drogue deploy condition as a function of the navigation accelerometer bias multiplier for each algorithm. Figure 22 shows a zoomed in view of the same data. Results from this study are harder to read, but PredGuid shows less overall sensitivity to the navigation acceleration bias than NSEG.

*5. Mass Properties*

- **Mass**

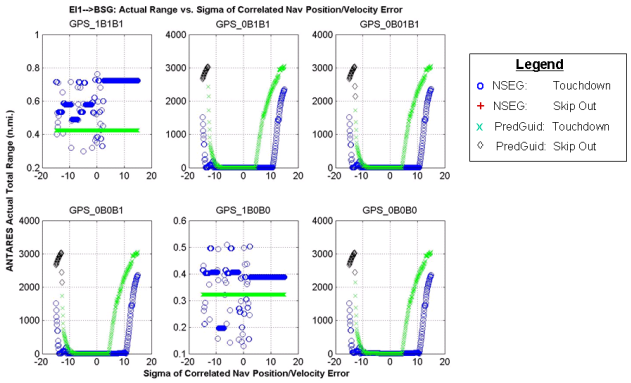


**Figure 17. Sensitivity to Correlated EI Position/Velocity Nav Error.**

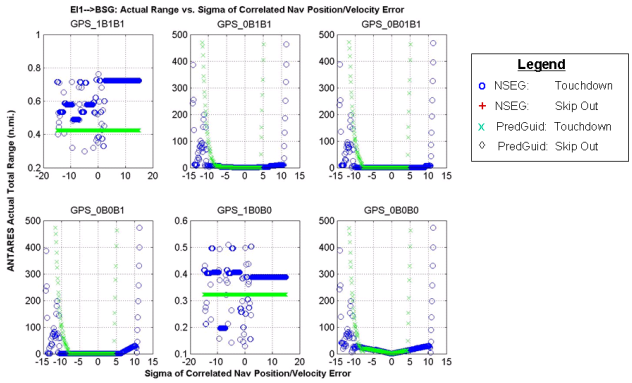


**Figure 18. Sensitivity to Correlated EI Position/Velocity Nav Error – Zoom 500 n.mi.**

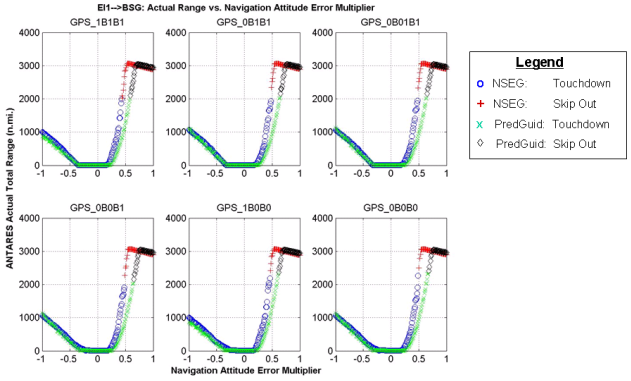


**Figure 19. Sensitivity to Navigated Attitude Error**

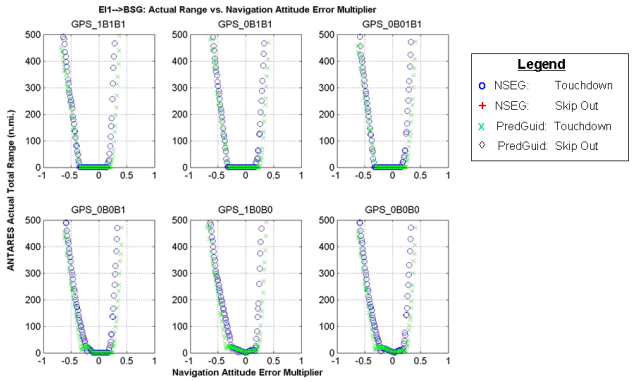


**Figure 20. Sensitivity to Navigated Attitude Error – Zoom 500 n.mi.**

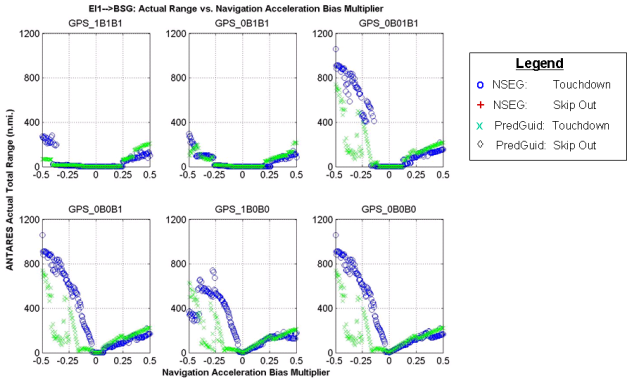


**Figure 21. Sensitivity to Navigation Accelerometer Bias**

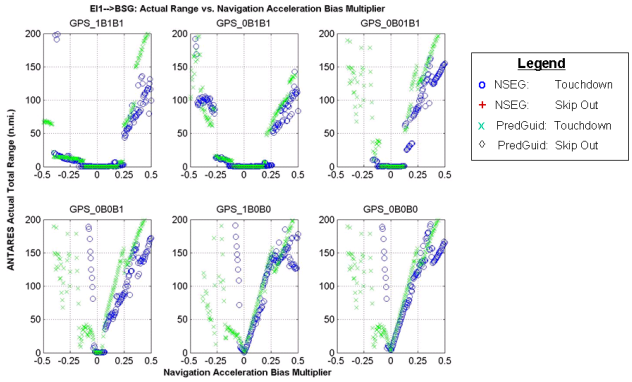


**Figure 22. Sensitivity to Navigation Accelerometer Bias – Zoom 200 n.mi.**

Figure 23 shows the total range-to-target at the drogue deploy condition as a function of the mass variation. From the figure it can be seen that neither algorithm is highly mass sensitive.

- **Center-of-Gravity**

  In Figure 24, the colors represent the total range-to-target at the drogue deploy condition for a given Y-body CG and Z-body CG location. The hypersonic L/D lines are superimposed on the plot for each

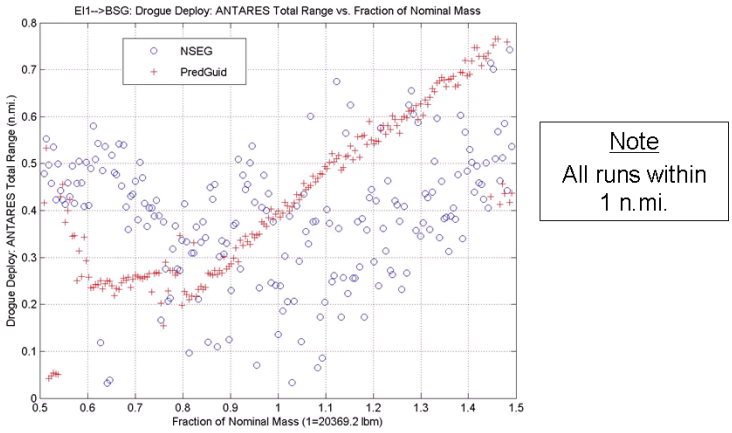


**Figure 23. Sensitivity to Mass.**

Z-body CG location. In Figure 25, the 2.7 n.mi. miss line and the 100 n.mi. miss line for each algorithm were co-plotted for easier comparison. In each plot, a cross marks the nominal CG location, and a box around the cross marks the expected 3-sigma variation box. It can be seen that this parametric study varied the CG location well outside its expected dispersion.

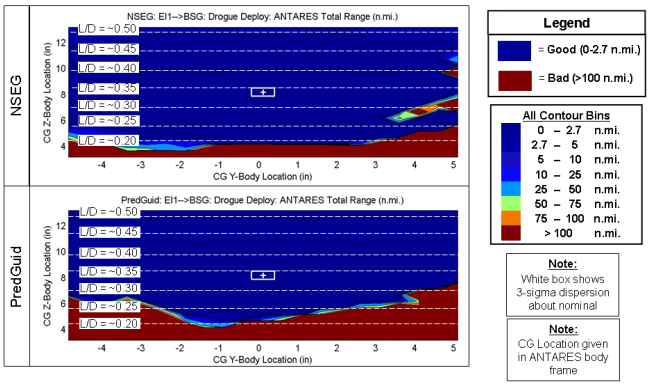


**Figure 24. Sensitivity to Center-of-Gravity.**

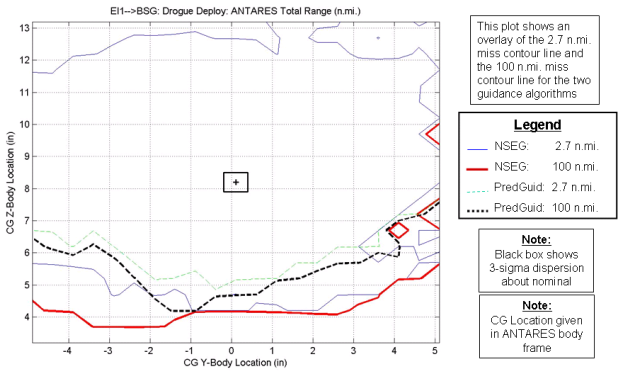


**Figure 25. Sensitivity to Center-of-Gravity Comparison.**

### *6. Atmosphere*

The following plots show the sensitivity to atmospheric variations for each algorithm. Figure 26 shows the total range-to-target at the drogue deploy conditions for NSEG. Note that NSEG has one small miss in January for an RPSCALE factor of 2.0. Figure 27 shows the total range-to-target at the touchdown conditions for NSEG. Figure 28 shows the total range-to-target at the drogue deploy conditions for PredGuid. Note that PredGuid hits the target for all months and RPSCALE values. Figure 29 shows the total range-to-target at the touchdown condition for PredGuid. Comparing the touchdown conditions between NSEG and PredGuid, it can be seen that the spread is roughly equivalent. This is probably due to the fact that PredGuid tends to deploy the chutes at a higher altitude than NSEG, thus allowing for more drift while under the chutes.

### *7. Control*

The following plots show the sensitivity to RCS thrust magnitude and control lag variations for each algorithm.

- **RCS Thrust Magnitude**

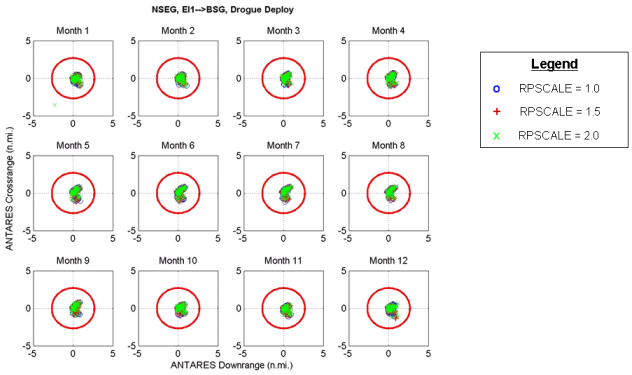


**Figure 26. Sensitivity to Atmospheric Variations - NSEG, Drogue Deploy.**

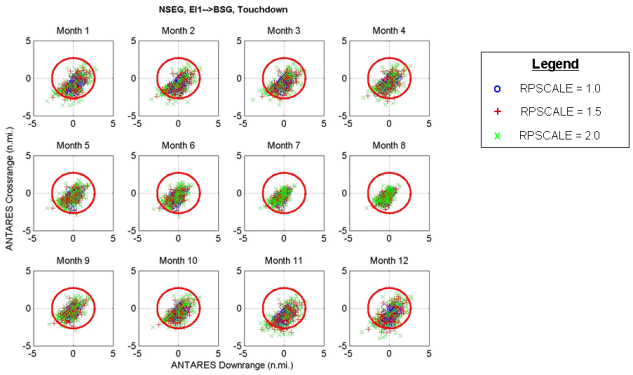


**Figure 27. Sensitivity to Atmospheric Variations - NSEG, Touchdown.**

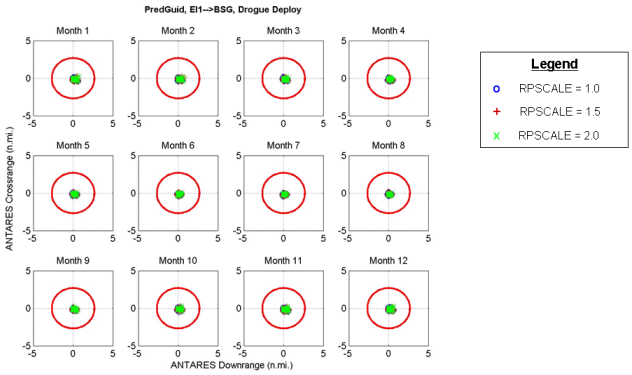


**Figure 28. Sensitivity to Atmospheric Variations - PredGuid, Drogue Deploy.**

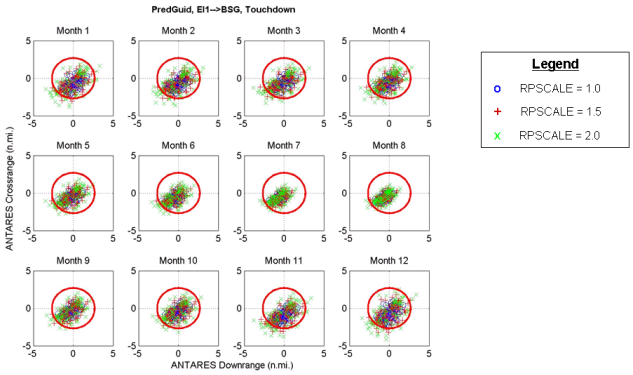


**Figure 29. Sensitivity to Atmospheric Variations - PredGuid, Touchdown.**

Figure 30 shows the total range-to-target at the drogue deploy condition as a function of the RCS thrust magnitude variation. Both algorithms break at an RCS thrust magnitude around 60 lbf. This assumes a single-string RCS system.

- **Control System Lag**

  Figure 31 shows the total range-to-target at the drogue deploy condition as a function of the control system lag variation. It can be seen that NSEG has an advantage over PredGuid in this category.

### *8. Aerodynamics*

The following plots show the sensitivity to aerodynamics of the vehicle for each algorithm. Figure 32 shows the NSEG total range-to-target at drogue deploy as a function of $C_L$ and $C_D$ uncertainty multiplier for each EI condition and $C_m$ uncertainty multiplier. Figure 33 shows the same data for PredGuid. One note of interest in Figure 33: In the first row, there are white bands running at low values of $C_L$ uncertainty multiplier. These are cases where PredGuid dropped into an infinite loop. For purposes of this study, the PredGuid infinite loop cases were treated as a miss. Figure 34 shows the AFOM for each $C_m$ uncertainty multiplier and EI condition for both NSEG and PredGuid. Figure 35 shows the difference between the AFOM (NSEG AFOM - PredGuid AFOM).

## V. Conclusion

Detailed six degree-of-freedom analysis has been conducted on two skip guidance algorithms. This analysis validates the feasibility of using a Skip-Entry guidance algorithm to access long-range targets up to 5,300

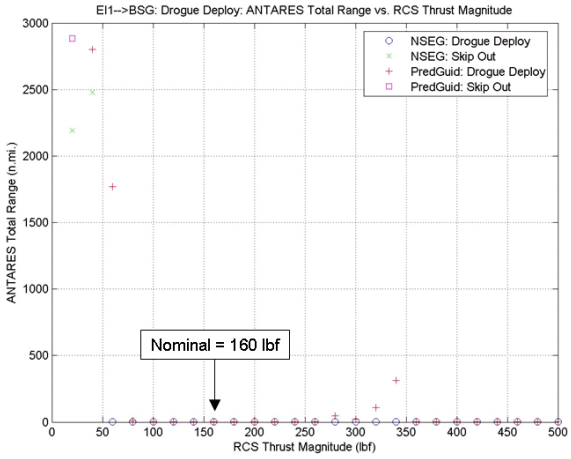


**Figure 30. Sensitivity to RCS Thrust Magnitude.**

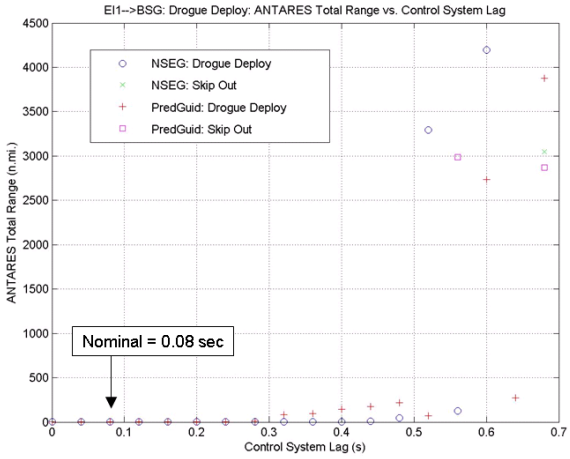


**Figure 31. Sensitivity to Control System Lag .**

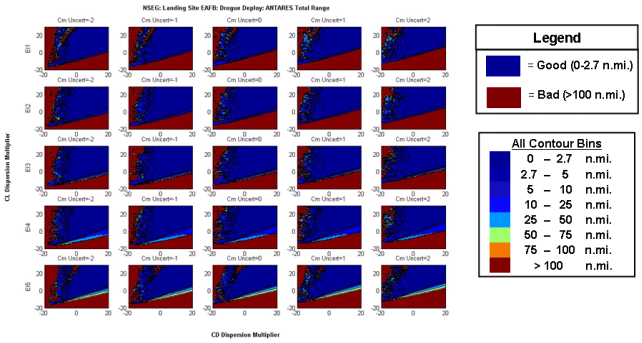


**Figure 32. Sensitivity to Aerodynamics, NSEG.**

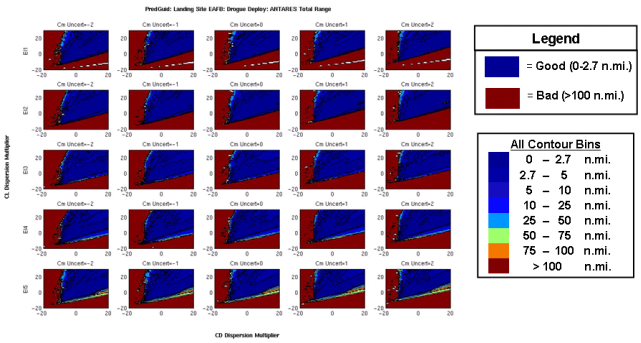


**Figure 33. Sensitivity to Aerodynamics, PredGuid.**

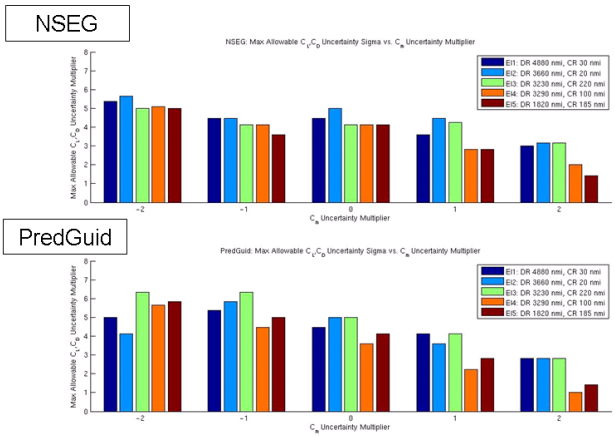


**Figure 34. Aerodynamic Figure-of-Merit for each algorithm.**

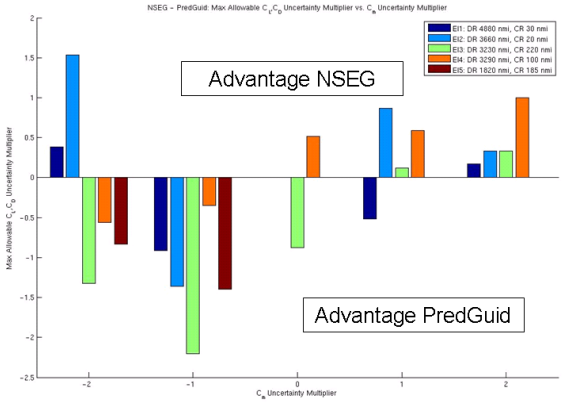


**Figure 35. Aerodynamic Delta Figure-of-Merit.**

nmi from EI without the use of a propulsive exo-atmospheric correction maneuver. This Skip-Entry range capability enables lunar return access to primary and weather alternate CONUS landing sites throughout the lunar-month cycle for the Moon at maximum declination.

The comparative guidance performance data shown in this report was provided to a senior selection board

tasked with recommending a primary and alternate Skip-Entry guidance algorithm. The PredGuid guidance algorithm was recommended as primary. As shown in this report, the PredGuid algorithm demonstrated overall better performance in Phase II of the guidance Merger activity in most categories. The NSEG algorithm will be maintained as the back-up algorithm and comparisons will be periodically performed to ensure that the optimum characteristics of both algorithms are identified and incorporated into the final flight skip entry guidance algorithm.

The estimated Technology Readiness Level (TRL) of the Skip-Entry guidance algorithms is currently still low for lunar return Skip-Entry flight. However, since these guidance algorithms are built upon the final phase Apollo guidance algorithm, the estimated TRL to support lunar return Direct Entry flight is much higher. In addition, recent analysis has indicated the possibility of using the PredGuid and NSEG guidance algorithms to support International Space Station (ISS) entry flight, with increased robustness offered by the guidance algorithm numerical "front-ends". Therefore, the possibility to leverage off ISS missions to increase the TRL of the proposed guidance algorithms to support lunar return is afforded.

### A. Guidance Improvements

Several areas have been identified within skip guidance where significant improvements in performance and robustness may be achieved.

#### *1. Managing Energy and Mode Transitions*

Work has recently been completed at Draper on a significant enhancement to the PredGuid skip entry guidance algorithm. This enhancement is based on a redesign of the energy management system and phase transition logic. A model-based predictor has been developed to determine the type of trajectory that is necessary to cover the target range and the appropriate time to transition to the next flight mode based on the trajectory type. The direct entry capability has been improved and expanded by incorporating a variable constant drag policy to manage energy, and by designing specific direct entry reference trajectories which are used by the path-following controller in the final descent phase. In addition, an intermediate loft regime is introduced to bridge the range capability between direct and skip entries. These upgrades to the PredGuid algorithm greatly improve its robustness to uncertainties encountered through the entry.

#### *2. Improved Lateral Logic*

The two guidance algorithms compared in this report use the Apollo strategy for managing crossrange. This strategy assumes that the energy/longitudinal channel can be managed independently from the lateral/crossrange channel. For vehicles with significant performance margin or low crossrange requirements, this is an excellent strategy. However, if performance margin is low or the vehicle is required to fly near its crossrange capability limit, negative interaction effects between the energy and lateral channels begin to appear. Currently, these interaction effects have been mitigated through tuning by the guidance designers. However, this solution provides minimal robustness. Several options exist that may provide significant benefit to skip entry guidance. They include a lateral channel predictor that could be used to control the number and time of bank reversals to ensure no adverse interactions with the energy channel, a fully coupled predictor-corrector in guidance that merges the lateral and energy channel, as well as simple analytic upgrades to the Apollo Lateral Logic as currently implemented. These potential modifications may significantly increase robustness and aid in RCS fuel management.

## Acknowledgments

Many people have worked on the technology which has made skip entry possible. The authors would like to recognize the technical achievements of the original Apollo engineers. For their significant contributions to this paper and to skip guidance, the authors would like to thank the following people: Mike Tigges, Tim Crull, Gregg Barton, Andrew Barth, and Travis Bailey.

## References

[1]Morth, R., "Reentry Guidance for Apollo," MIT/IL R-532 Vol. I, 1966.

[2]Moseley, P. E.; Morris, R. L., "The Apollo Entry Guidance: A Review of the Mathematical Development and its Operational Characteristics," Task MSC/TRW A-220, Dec. 1969.

[3]McCleary, B.; Crull, T.; Schmitt, L.; Wood, R., "Lunar Return Footprint Assessment Using Apollo Guidance," McDonnell Douglas Space Systems Company, Houston Division, Guidance Navigation & Control Internal Report, Feb. 1992.

[4]DiCarlo, J. L., "Aerocapture Guidance Methods for High Energy Trajectories," S. M. Thesis, Department of Aeronautics and Astronautics, Massachusetts Institute of Technology, June 2003.

[5]Bairstow, S. H., "Reentry Guidance with Extended Range Capability for Low L/D Spacecraft," S. M. Thesis, Department of Aeronautics and Astronautics, Massachusetts Institute of Technology, February 2006.

[6]Bairstow, S. H, Barton, G., "Orion Reentry Guidance with Extended Range Capability Using PredGuid," AIAA-2007-6427, August 2007.

[7]Hoelscher, Brian R., "Orion Entry, Descent, & Landing Simulation," AIAA-2007-6428, August 2007.

[8]Orion Vehicle Simulation Data Book, Preliminary Issue, Revision A, CEV-MA-07-003, Lockheed Martin Space Systems Company, Denver, Colorado, April 2007.

[9]CAP Aeroydnamics Team, "Orion Aerodynamic Databook, Ver 0.2", NASA JSC-63402, CXP-72167, January 2007.

[10]CAP Aerodynamics Team, "Formulation of the Orion Aerodynamic Database, Revision 0.2.5", EG-CEV-06-37, February 2007.

[11]CAP Aerodynamics Team, "CEV Aerotab Database API Users Guide, Rev 0.2.1", January 2007.